#### **Research Article**

Jiuyang Li, Zhenwei Wang\*, Jinpeng Guo, Jingwei Luo, Xinmei Fan, and Yuepeng Zhu

# Study on physical and mechanical properties of complex-phase conductive fiber cementitious materials

https://doi.org/10.1515/rams-2024-0041 received January 29, 2024; accepted June 05, 2024

**Abstract:** With the continuous upgrading of infrastructure construction and the gradual development of theoretical research about engineering construction, higher performance requirements have been put forward for concrete materials. Therefore, to meet the engineering quality requirements of various concrete structures, the research direction of engineering materials has shifted towards developing new concrete with high strength, high ductility, high toughness, and other multifunctional properties. Mixing two or more types of fibers with conductive properties with the cement matrix material allows various fibers to leverage their strengths and weaknesses, thereby utilizing their respective characteristics. This results in the formation of a complexphase conductive fiber cementitious material (CFCM), which enhances the safety, durability, and toughness of the structure. It enables the engineering structure to exhibit intelligence and resourcefulness, thereby improving its service life and reducing the full life cycle cost of the cementitious material structure. Additionally, this approach relatively eases the demand for concrete materials and reduces material consumption. This method represents one of the research directions for new concrete. Complex-phase CFCMs are essentially smart materials capable of sensing not only compressive or tensile stresses but also temperature. The emergence of CFCM represents a significant step forward in enhancing the mechanics, functionality, and sustainability of modern infrastructure. In this experiment, an orthogonal test involving 16 working conditions with three factors and four levels

was designed, with steel fiber (SF) type, SF content, and carbon fiber (CF) content as the factors. The study focused on the physical and mechanical properties of composite conductive fiber cement-based materials containing both SF and CF. Performance indicators such as flexural strength, volume resistivity, and energized temperature rise of the composite conductive fiber cement-based materials were tested. The analysis of orthogonal tests produced the following results regarding the degree of influence of each factor on the mechanical and physical properties: the order of influence on flexural strength was SF doping > SF type > CF doping. Further analysis revealed that the best combination was A4B4C4. The relationship between the effect of each factor on resistivity is as follows: carbon fiber doping > SF doping > SF type. Comparing the weights between the levels, it can be observed that the optimal combination of conductivity schemes is also A3B4C4. SF and CFs, respectively, enhanced the mechanical and physical properties of complex-phase conductive fiber cementitious materials. The results of the temperature rise test on cementitious materials concluded that there is a certain relationship between the temperature rise and electrical conductivity. Specifically, the higher the electrical conductivity, the greater the temperature rise observed. Through orthogonal analysis of electrical conductivity, disregarding the effect of the non-significant influence factor SF type on the conductive heating test, the impact of two factors, CF doping and SF doping, on the heating test was investigated under 16 sets of conditions, and the data were analyzed visually. The optimal mix ratio for the test is A3B4C4, determined through comprehensive optimization of orthogonal and intuitive analyses. This means that the optimal physico-mechanical properties are achieved when using copper-plated SFs, with a SF dosage of 1.25% and a CF dosage of 0.48%. As a preceding study in the field of intelligent concrete, this experiment explores the research path of intelligent concrete, which holds positive significance for subsequent, more intricate research endeavors.

Changchun Institute of Technology, Changchun, 130012, China, in e-mail: 942482763@qq.com su

\* Corresponding author: Zhenwei Wang, School of Civil Engineering,

**Jiuyang Li, Jinpeng Guo, Jingwei Luo, Xinmei Fan, Yuepeng Zhu:** School of Civil Engineering, Changchun Institute of Technology, Changchun, 130012, China

**Keywords:** cementitious materials, steel fibers, carbon fibers, mechanical properties, physical properties

#### 1 Introduction

Concrete stands as a foundational building material integral to the construction of civil engineering projects, including roads, bridges, and residential structures. Its indispensable role underscores its significance in the realm of construction, forming the essential core of diverse infrastructure developments. In recent years, as society has rapidly developed and progressed, the inadequacy of traditional cementitious materials with single functional properties has become apparent. These materials struggle to meet the demands of multifunctional engineering needs and address the challenges posed by the ongoing technological revolution. The evolving landscape necessitates a reevaluation and advancement in cementitious materials to align with contemporary engineering requirements and adapt to the changing dynamics brought about by the new technological era. In contemporary times, the concept of "smart materials" has garnered widespread attention across various spheres of society. The incorporation of these "smart materials" into engineering materials, particularly concrete, imparts distinctive qualities such as self-perception, self-regulation, self-repair, and self-adaptation. This transformative integration elevates conventional concrete to the realm of "smart concrete," reflecting advancements that align with the principles of self-awareness and adaptive functionality. Currently, numerous physical and mechanical properties of smart concrete have become a prominent research topic. This burgeoning area of study reflects the heightened interest and significance in exploring the characteristics and capabilities of smart concrete in today's research landscape. Among these, conductive fiber concrete serves as the cornerstone of intelligent concrete. It constitutes a concrete matrix incorporating one or more "smart materials" (conductive fibers) as filler materials, resulting in the formation of conductive composite materials [1-4]. In ordinary concrete under normal conditions, the resistivity typically falls within the range of  $10^6$ – $10^9$   $\Omega$ ·cm. However, when incorporating "smart materials" into the mix, such as conductive concrete, the resistivity can be reduced to below  $10^4 \,\Omega$  cm [5]. These conductive materials include steel fibers (SFs) [6-8], steel slag [9,10], CFs [11], carbon nanotubes [12,13], graphene [14,15], carbon black [16], and others. Conductive concrete, characterized by robust electrical conductivity, has already found application in engineering for functions related to both electrical and thermal conductivity. This versatile material serves various purposes in relevant fields, showcasing its potential for practical use [17]. With the increasing maturity of research on the mechanical properties of SF cementitious composites, there has been a gradual increase in research on their electrical and thermal properties as well. However, SFs are prone to surface

corrosion and passivation in the highly alkaline environment of the cementitious matrix. This leads to a gradual decrease in the electrical conductivity of conductive cementitious composites with age. Therefore, considering the excellent strength of SFs and their good electrical conductivity, an increasing number of scholars are incorporating an appropriate amount of SFs and other conductive phases into cementitious materials. This approach allows for the preparation of composite materials that not only meet the requirements for higher strength but also ensure the stability of electrical conductivity in conductive cementitious composites. Guan et al. [18] incorporated smart concrete materials, specifically short-cut CFs. into the concrete mix. Their findings revealed an increase in tensile strength and demonstrated good sensitivity to temperature and stress. Li et al. [19,20] conducted a study on on-site snow melting, ice melting, and laboratory de-icing using CF conductive concrete panels. The study results demonstrated that the heat generated by conductive CF concrete effectively melts the snow on the road surface. As a consequence, CF concrete exhibits high temperature sensitivity. When an electric field is applied to CF concrete, it induces a thermoelectric effect, commonly referred to as the electrothermal effect, within the concrete. Hence, CF conductive concrete finds application in projects such as bridge pavements, airport runways, and plant roofs. Leveraging the electric heat effect, it achieves automatic snow melting and de-icing, offering a greener, more efficient, and feasible method. This approach aligns with China's principles of green and sustainable development.

In the study of conductive cementitious materials, several factors need consideration, including the resistivity of the conductive material, cost, dispersion, and others. For instance, carbon nanotubes exhibit excellent electrical conductivity, mechanical strength, and thermal stability. When used as a conductive phase additive in materials, they can effectively reduce the electrical resistivity of concrete, providing more stable resistance data. However, their application in projects is constrained by cost considerations [21]. Graphite and carbon black are easily obtainable and costeffective materials, exhibiting excellent electrical conductivity and serving as high-quality electrically conductive fillers. The particle size distribution of carbon black influences its electrical conductivity. However, excessively high graphite content in concrete may adversely impact the mechanical properties of the material [22,23]. Carbon nanotubes, carbon nanofibers, carbon black nanoparticles, and graphite all fall under the category of conductive phase materials at the carbon nanoscale, characterized by a substantial specific surface area. However, their dispersion in the concrete mixing process poses a challenge due to their nanoscale dimensions. CF possesses commendable electrical,

thermal, and mechanical properties, and it is more conducive than graphite for forming a conductive network within the concrete. Consequently, CF concrete exhibits superior conductive properties compared to graphite concrete. As domestic CF production technology matures and experiences rapid growth, CF is no longer reliant on imports. This development has led to a significant reduction in the preparation costs of CF conductive concrete. SFs contribute to favorable electrical and mechanosensitive properties in concrete [6,7,24]. The incorporation of both CF and SF in concrete not only leads to a significant improvement in mechanical properties, durability, and impact resistance but also facilitates the interlacing of fibers within the concrete, forming a staggered conductive network. This arrangement further enhances electrical conductivity.

To meet the engineering specifications for conductive concrete, factors such as electrical conductivity, mechanical properties, and electro-thermal effects must be taken into account. The incorporation of conductive phase materials into cementitious materials serves to enhance the mechanical, electrical, and thermal properties of cementitious composites, all while preserving structural integrity. Conductive fiber mortar not only serves as a research foundation for cement-based materials but also functions as a material for snow and ice melting on roads. In addition to requiring mechanical strength and conductive stability, it should exhibit excellent electrical and thermal conductivity. Belli et al. [25] conducted a study wherein SFs were incorporated into mortar to investigate its physical properties and electrical conductivity. The findings revealed a notable enhancement, with the tensile and flexural strength of the mortar increasing by 100% following the inclusion of SFs. Moreover, this incorporation resulted in a reduction in the resistivity of the mortar by one order of magnitude. Reza et al. [26] discovered that the tensile strength of CF reinforced mortar, with a volumetric fraction of 0.6%, increased by approximately three times compared to normal mortar. Chiarello and Zinno [27] conducted an investigation into the electrical conductivity of CF-reinforced cement composites. They analyzed various factors influencing it, including fiber volume fraction, fiber length, hydration time, and sand-cement ratio. The results demonstrated that the addition of a small quantity of CFs to the cement mortar substantially increased the electrical conductivity of the material. In contrast, scholars such as Li and Wang [28], Ba and Gao [29], Huang et al. [30], and Chen and Chung [31] discovered that the inclusion of CFs led to a reduction in the compressive strength of cementitious materials. The phenomenon wherein conductive cementitious materials generate heat when energized is referred to as the electrothermal effect, also known as the Joule effect.

Resistivity emerges as the primary factor influencing the thermal power of conductive fiber mortar composites. Under constant voltage conditions, materials with different resistivities exhibit varying heating powers.

Hence, formulating conductive mortar with excellent electrical conductivity holds great significance for its widespread application in engineering. In this study, building upon prior research, an experimental study was conducted to investigate the compounding of SF and CF on the mechanical properties, electrical conductivity, and electro-thermal effects of cement mortar. The objective is to explore the potential application of fiber conductive mortar in the snow and ice melting operations of overpasses, platforms, pavements, and other pavement structures in the cold regions of the northeast.

#### 2 Test materials and experimental design

#### 2.1 Test materials

The required raw materials for this test primarily include concrete matrix components (cement, sand), conductive phase materials (SFs, CFs), and admixtures (water-reducing agent, dispersant, defoamer). The cement used is ordinary silicate cement (P.O42.5) manufactured by Jilin Yatai Group Yitong Cement Co., Ltd. Its physical properties and chemical composition comply with the specifications outlined in the General Silicate Cement standard (GB175-2020) [32]. Medium sand with a fineness modulus of 2.61 is chosen as the sand component, meeting the specifications outlined in the Standard for Quality and Inspection Methods of Sand and Stone for Ordinary Concrete (JGJ 52-2006) [33]. The water-reducing agent produced by Hongxiang Building Admixture Factory in Laiyang City, Shandong Province was selected for the test. Hydroxyethyl cellulose (HEC) and tributyl phosphate (chemical molecular formula C<sub>12</sub>H<sub>27</sub>PO<sub>4</sub>) were chosen as the dispersant and defoamer, respectively, for the test.

The test utilized four types of SFs (shear, milled pin type, copper-plated type, end-hook type) produced by Hengshui Maurer Metal Products Co. Ltd, designated as SFA, SFB, SFC, and SFD, respectively, as shown in Figure 1. The basic properties are detailed in Table 1, and they conform to the standard test for Steel Fiber for Concrete (GB/T 39147-2020) [34].

The CF selected for the test, manufactured by Toray Carbon Fiber (Guangdong) Limited Liability Company, is

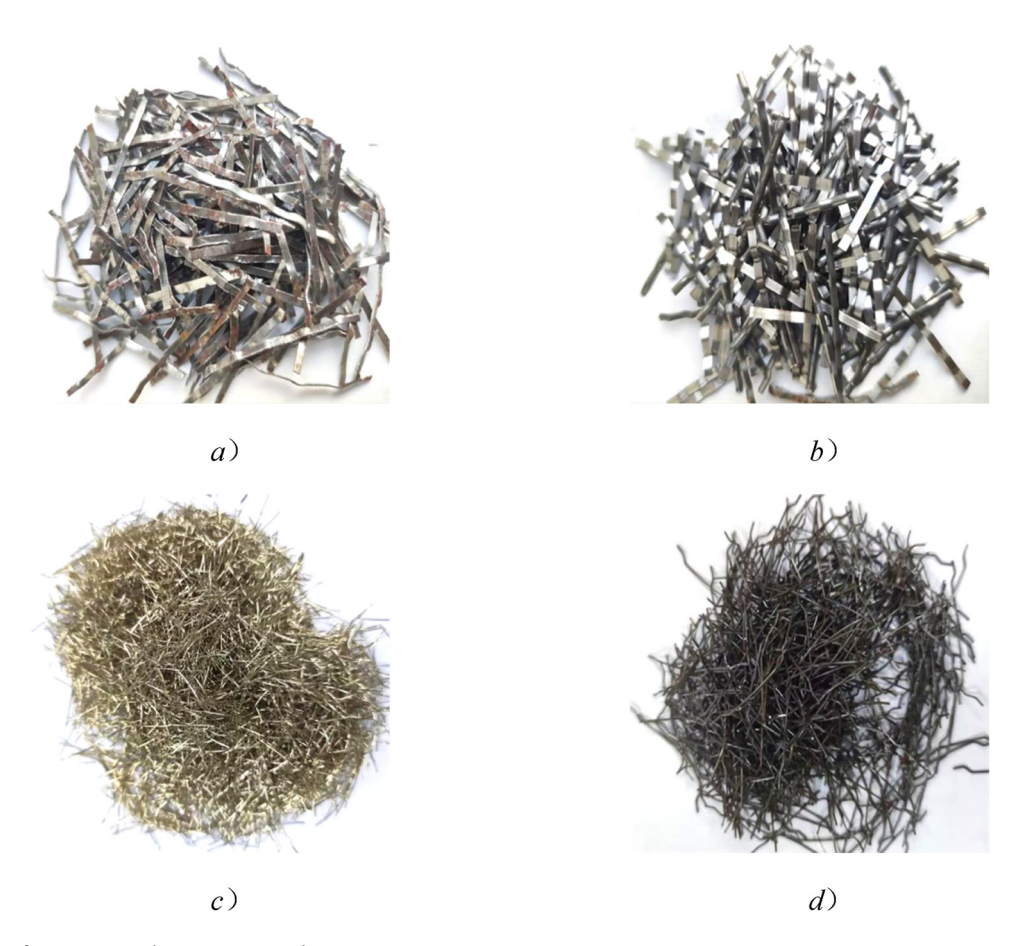


Figure 1: Types of SFs. (a) SFA. (b) SFB. (c) SFC. (d) SFD.

depicted in Figure 2, and its fundamental properties are detailed in Table 2.

#### 2.2 Experimental design

#### 2.2.1 Base mix for cementitious materials

In this test, cement, sand, water, and water reducer were utilized as test materials to prepare cementitious materials with a matrix water-cement ratio of 0.49. The baseline mix ratios for the cementitious material are presented in Table 3.

#### 2.2.2 Orthogonal experimental design

In 2012, Yuan [35] conducted a study on the piezoelectric properties of CF concrete. The best pressure-sensitive properties were achieved when the composite was externally doped with 0.5% CFs. In 2020, Wang *et al.* [36] conducted a study on the compressive strength, flexural strength, resistivity, and pressure-sensitive properties under monotonic loading for hybrid fiber reactive powder concrete with varying amounts of SF and CF. The results indicate that concrete with a steel fiber content of 1% and CF content of 0.5% exhibits higher mechanical strength and excellent pressure sensitivity. In order to obtain better mechanical

Table 1: SF performance index

Performance indicators	Sheared steel fiber (SFA)	Milled pinned steel fiber (SFB)	SF copper plated (SFC)	End hooked SF (SFD)
Fiber length (mm)	38	32	13	35
Tensile strength (MPa)	450	720	2,850	1,150



Figure 2: Carbon fiber.

and electrical properties, the SF and CF are selected according to the volume of doping, in which the doping of the four SFs is 0, 0.35, 0.65, 0.95, and 1.25%; CF doping is 0, 0.12, 0.24, 0.36, and 0.48%. Two types of fibers, SFs and CFs, were compounded and blended into cementitious materials to prepare complex-phase conductive fiber mortar. A threefactor, four-level orthogonal test was designed to investigate the electrical conductivity, flexural strength, and electrical and thermal properties of complex-phase conductive fiber mortar. Four different fiber dosages were designated as design levels, utilizing SF type, SF dosage, and CF dosage as the test factors. Sixteen groups (48) of standard mortar specimens, each with dimensions of  $40\,\mathrm{mm}$  ×  $40\,\mathrm{mm}$  × 160 mm, were fabricated. The dosage of complex-phase conductive fibers is detailed in Table 4. Among them, SF and CF represent steel fibers and carbon fibers, respectively. A, B, C, and D represent four types of SFs (shear, milled pin, copperplated, and end-hooked), and the numbers after the letters represent the volume doping of conductive fibers. For example, SFA125 represents the shear-type SF with a volume dosage of 1.25%, and CF24 represents the CF with a volume dosage of 0.24%. HEC and tributyl phosphate are used as the dispersant and antifoam agent in this test, with selected dosages of 0.4 and 0.03% of the total mass of the cementitious material, respectively.

#### 2.3 Test methods

#### 2.3.1 Mechanical property tests

Since the flexural strength of SF cementitious composites is significantly higher than that of cementitious sand specimens without SFs, ordinary flexural testing machines are

 Table 2: Basic performance parameters of CF

er diameter (µm)	Standard length (mm)	Heap density (g·cm <sup>-3</sup> )	Carbon content (%)	) Tensile strength (MPa) Tensile modulus (GPa) Density (g·cm <sup>-3</sup> )	Tensile modulus (GPa)	Density (g·cm <sup>-3</sup> )	Resistivity (Ω·cm)
	8	0.4	76	3,530	230	1.76	1.0–1.3

6 — Jiuyang Li et al. DE GRUYTER

Table 3: Cement mortar base mix ratio

Raw materials	Clinker	Sand	Water	Water reducing agent
Dosage (kg·m <sup>-3</sup> )	450.00	627.00	176.00	0.9

unable to fully fracture them. The mechanical specimens in this study all of the dimension 40 mm × 40 mm × 160 mm, and their flexural strength tests are conducted using the three-point bending loading method. Prior to the test, the load application position on the specimen was marked. Subsequently, the specimen was positioned on the flexural testing machine according to the correct placement, and the flexural strength of the cement mortar was conducted in accordance with the relevant provisions and requirements outlined in the "Polymer-modified Cement Mortar Test Procedure" (DL/T 5126-2021) [37]. The formula for flexural strength is presented in Eq. (1), and the results are accurate to 0.01 MPa.

$$f_{\rm b} = \frac{1.5PL}{b^3},\tag{1}$$

where  $f_b$  is the flexural strength (MPa), P is the destructive load (N), L is the distance between supporting cylinders (mm), and b is the side length of prismatic square section (mm).

After calculating the flexural strength value of each specimen, the average of the flexural strength values of a



Figure 3: Flexural strength test.

group of three specimens shall be taken as the test result. If there are three flexural strength values exceeding ±10% of the average value, those values should be excluded. The average value of the remaining two values will then be considered as the final test result for flexural strength. The schematic diagram of the three-point bending loading is shown in Figure 3.

#### 2.3.2 Conductivity test

The voltammetric resistance can be categorized into internal and external methods. Due to the significantly higher resistance value of conductive fiber cement-based material compared to

Table 4: Complex phase conductive fiber doping and orthogonal test factor level table

Test conditions		SF		CF	
	Factor (A)	Factor (B)		Factor (C	)
	SF types	Mass admixture (kg·m <sup>-3</sup> )	Admixture (%)	Mass admixture (kg·m <sup>-3</sup> )	Admixture (%)
L-1	1 (SFA)	27.3	1 (0.35)	2.12	1 (0.12)
L-2	1 (SFA)	50.7	2 (0.65)	4.24	2 (0.24)
L-3	1 (SFA)	74.1	3 (0.95)	8.48	3 (0.36)
L-4	1 (SFA)	97.5	4 (1.25)	16.96	4 (0.48)
L-5	2 (SFB)	27.3	1 (0.35)	4.24	2 (0.24)
L-6	2 (SFB)	50.7	2 (0.65)	2.12	1 (0.12)
L-7	2 (SFB)	74.1	3 (0.95)	16.96	4 (0.48)
L-8	2 (SFB)	97.5	4 (1.25)	8.48	3 (0.36)
L-9	3 (SFC)	27.3	1 (0.35)	8.48	3 (0.36)
L-10	3 (SFC)	50.7	2 (0.65)	16.96	4 (0.48)
L-11	3 (SFC)	74.1	3 (0.95)	2.12	1 (0.12)
L-12	3 (SFC)	97.5	4 (1.25)	4.24	2 (0.24)
L-13	4 (SFD)	27.3	1 (0.35)	16.96	4 (0.48)
L-14	4 (SFD)	50.7	2 (0.65)	8.48	3 (0.36)
L-15	4 (SFD)	74.1	3 (0.95)	4.24	2 (0.24)
L-16	4 (SFD)	97.5	4 (1.25)	2.12	1 (0.12)

the resistance value of the voltmeter and ammeter, employing the external method with a large voltmeter shunt introduces substantial test errors. Conversely, the internal method with a small ammeter shunt minimizes test errors, resulting in highly accurate data measurements. Therefore, the internal method is preferred for measuring the resistance of conductive fiber cement-based material. The circuit diagrams for the internal and external connection methods are depicted in Figure 4.

For the two-electrode voltammetry measurement of resistance, the principle equation for the derivation of Ohm's law formula, expressing the relationship between voltage, current, and resistance, is illustrated in Eq. (2).

$$R = \frac{U}{I}. (2)$$

Based on the measured resistance values, the resistivity of the tested parts is calculated using the volume resistivity formula (3).

$$\rho = \frac{RA}{L},\tag{3}$$

where  $\rho$  is the resistivity ( $\Omega$ ·m), R is the resistance value  $(\Omega)$ , L is the electrode spacing (m), and A is the cross-sectional area (m<sup>2</sup>).

A digital multimeter served as an ammeter connected in series to the circuit to measure the current of the specimen during the test. Additionally, a current acquisition system was employed to transmit the electrical signal to the computer through a converter and record the change in the specimen current with time in real-time. The conductivity performance test is illustrated in Figure 7.

#### 2.3.3 Warming test

To investigate the warming pattern of specimens under energized conditions for various complex-phase conductive fiber mortars, this test applied a 64 V DC voltage to the specimens. The specimens were energized continuously for 120 min, during which the entire process involved collecting current

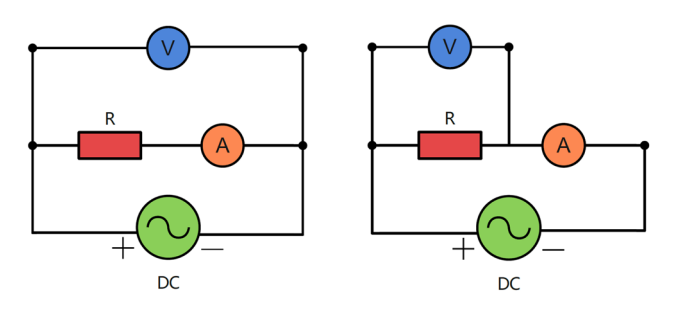


Figure 4: Circuit diagram of internal and external connection method.

data and monitoring temperature changes. To maintain a controlled test environment and prevent heat exchange with the surroundings, a custom-made insulation box using benzene insulation boards was employed.

In this study, the warming test is conducted based on electrical conductivity. The two-electrode method is employed to integrate the test block into the circuit. Monitoring of current and voltage is achieved by connecting the current collector and signal converter in series to the circuit. Real-time current collection is performed, and the data are recorded and saved. Oin [38] conducted resistance testing on the specimen using DC voltammetry. This method requires synchronizing the voltage and current on both ends of the specimen using the same frequency voltage collector and current collector. However, ensuring the synchronicity of the two collectors in practice is challenging, and the use of two collectors also increases costs. To address this issue, an RS485 converter was employed to collect the serial port data from the collector into an RS485 serial port. This setup enables direct connection with the computer for the conversion of electrical signals into digital signals, facilitating real-time monitoring and recording of data.

The test instruments utilized include a laptop computer, DC power supply, digital multimeter, HY004 collector, and RS485 converter. The connection scheme for receiving electrical signal data during the test is illustrated in Figure 5.

The test was conducted with the specimen energized for the collection of temperature data. The experimental apparatus used included a laptop computer, thermocouples, and a sheet-type temperature probe. Among these instruments, the use of a sheet-type temperature probe is preferred due to its ability to closely adhere to the specimen and its higher sensitivity to temperature changes. Detailed test connections with the K-type temperature sensor are depicted in Figure 6.

Liu [39] compared the accuracy and dispersion of the internally buried copper sheet electrode method with the pasted electrode method for measuring the resistance value of conductive fiber concrete. The results indicated that the resistance values obtained by the embedded copper sheet electrode method were significantly larger than those obtained by the paste electrode method. Although the error values of both groups are within the normal error tolerance, the paste electrode method exhibits better stability. Therefore, in this test, the paste electrode method was selected to conduct the conductivity and temperature rise performance test of the conductive fiber cementitious material. For the test setup, copper foil conductive tape is pasted on both ends of the test piece, and a voltage of 64 V (DC power supply) is applied for 2 h. Four sheet-type temperature probes are 8 — Jiuyang Li et al. DE GRUYTER



Figure 5: Data reception connection method.



Figure 6: Ramp-up test connection.

adhered to the specimen surface at the positions shown in Figure 6. While the power supply is active, temperature data are recorded every 1s for the temperature changes at the four positions on the specimen. The arrangement of the lamellar temperature probes and electrodes is depicted in Figure 7. Additionally, the temperature rise test process diagram and test schematic are illustrated in Figure 8.

#### 2.4 Specimen preparation

Measure the necessary masses of sand, cement, water reducer, CF, SF, dispersant, defoamer ( $C_{12}H_{27}PO_4$ ), and water according to the test design requirements and the mix ratio for the mortar test block. Initially, sand and cement are mixed and stirred for 30 s. Subsequently, SFs are added

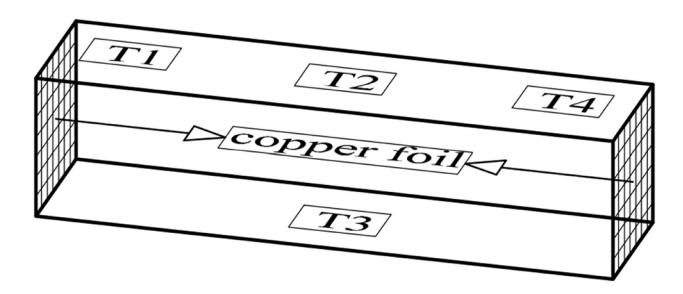
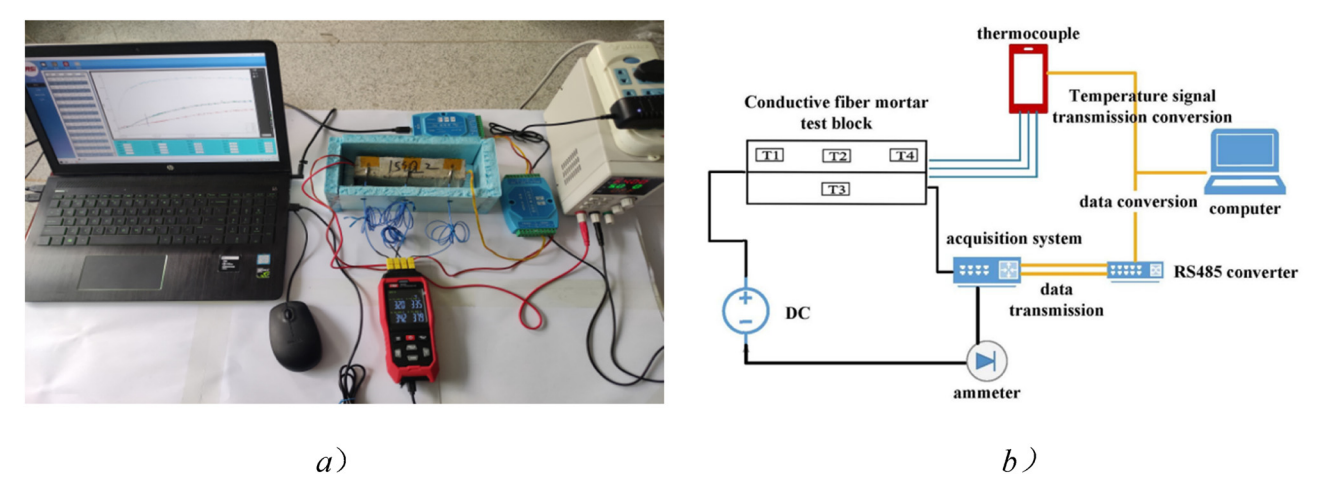


Figure 7: Temperature probe and electrode arrangement.

sequentially, and dry mixing is continued for 60 s to achieve a uniform mixture of each aggregate. Subsequently, the prepared CF dispersion, along with water and water-reducing agent solution, was poured into the mixer and continued to mix for 180 s. Upon completing the molding process, it is necessary to subject the mold to vibration on the vibration table. Simultaneously, a plastering knife should be used to smooth the surface of the specimen until the pulp on the surface of the specimen mold floats without the presence of excessive bubbles. Subsequently, the vibration table can be turned off. The specimen surface should then be covered with plastic wrap to maintain the humidity of the specimen. Finally, after placing the specimens in a room for 24 h, they can be demolded and numbered. After demolding, the specimens are placed in a standard curing room under specified conditions for 28 days. Upon completion of the curing period, the specimens are removed and placed on an indoor surface for 6 h to allow them to dry before conducting various performance tests. The CF dispersion method and preparation flowchart are illustrated in Figures 9 and 10.

# 3 Orthogonal test design and result analysis

The three analysis methods employed in the orthogonal test are range analysis, variance analysis, and matrix analysis. Practical application demonstrates that the range



**Figure 8:** Schematic diagram of the conductivity test experiment. (a) Mortar specimen electric heat test chart. (b) Schematic diagram of mortar specimen temperature sensitivity.

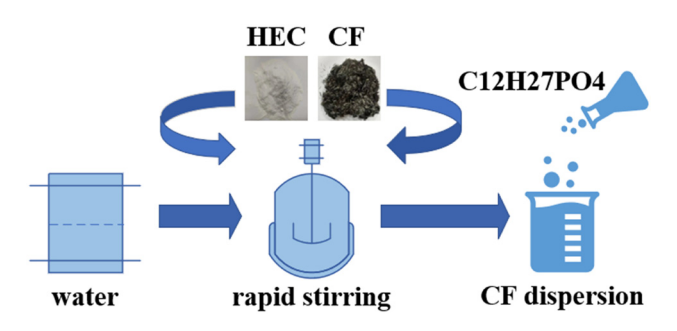


Figure 9: CF dispersion flow chart.

analysis method can present test data in a visually intuitive and clear manner. Through simple numerical calculations, results can be assessed, enabling the determination of primary and secondary factors, optimal levels, and optimal combinations resulting from experimental optimization. Variance analysis is a mathematical method used to differentiate between the differences in experimental results caused by changes in factor levels (or interactions) and the differences caused by error fluctuations. As one of the most fundamental methods of mathematical statistics,

variance analysis offers advantages such as simplicity, minimal calculation requirements, and easy dissemination. It serves as an effective tool for analyzing experimental data in scientific and production research. The above two methods are subject to varying degrees of influence from subjective factors during the analysis process. In contrast, matrix analysis is a relatively objective method for processing test data. By calculating the weight of each factor and level affecting the test results, the optimal combination scheme of the test can be determined.

### 3.1 Mechanical properties orthogonal test results

The research and analysis of the mechanical properties, specifically the flexural strength, of the complex-phase conductive fiber mortar primarily employed orthogonal test polar analysis, analysis of variance, and matrix analysis. This approach was utilized to investigate the impact of each factor on the flexural strength of the complex-

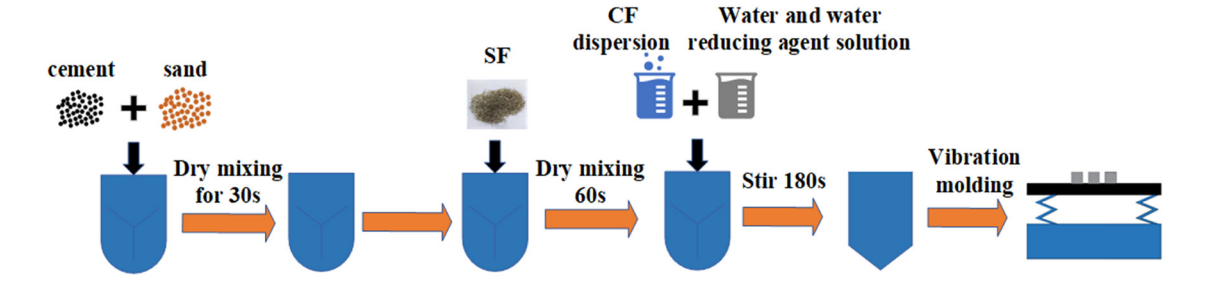


Figure 10: Flow chart for the preparation of complex phase conductive fiber cementitious materials.

Table 5: Summary of flexural strength test results of complex-phase conductive fiber mortar

Test conditions	Flexural strength (MPa)						
L-1	5.02	L-5	11.38	L-9	12.11	L-13	13.38
L-2	10.57	L-6	8.13	L-10	14.74	L-14	16.55
L-3	13.47	L-7	16.02	L-11	16.92	L-15	15.11
L-4	15.48	L-8	13.63	L-12	17.73	L-16	18.20

phase conductive fiber mortar, discerning the main and secondary influences. The analysis involved a comprehensive examination of the factors and levels, considering the test indicators, and culminating in the identification of the optimal combination of factors and levels. Table 5 provides a summary of the orthogonal test results for the flexural strength of complex-phase conductive fiber mortar.

#### 3.1.1 Flexural strength extreme variance analysis

The results of the flexural strength under the 28-days orthogonal test of complex-phase fiber mortar are presented in Figure 11. The test outcomes were subjected to polar analysis, and the results of the analysis are detailed in Table 6. In the table, L-1 represents the test conditions, and the information regarding fiber types and dosages for each group of conditions is presented in Table 4.

Table 6 presents the polar analysis results derived from the orthogonal test data for complex-phase conductive fiber mortar. The polar differences in the effect of SF type, steel fiber dosage, and CF dosage on the 28-days flexural strength of complex-phase conductive fiber mortar were 4.67, 5.79, and 2.84, respectively. The degree of influence of different factors on the 28-days flexural strength of complex-phase conductive fiber mortar specimens is ranked as follows: SF dosage > SF type > CF dosage. According to the orthogonal test results, it is evident that the SF dosage has the most significant effect on its flexural strength.

Table 6: Summary of the results of the analysis of extreme variance

Parameters	A (SF type)	<i>B</i> (SF dosage)	C (CF dosage)	Blank column
kı	11.14	10.47	12.07	13.83
k2	12.29	12.50	13.70	13.63
<i>k</i> 3	15.37	15.38	13.94	14.45
k4	15.81	16.26	14.90	12.71
Polar	4.67	5.79	2.84	1.74
deviation R				

To more clearly illustrate the impact of each factor on the flexural strength of complex-phase conductive fiber mortar specimens at different levels, a line graph depicting the average results obtained at each level is presented in Figure 12.

The influence of factor A (type of SF) on the flexural strength of mortar specimens is depicted in Figure 12. The end-hook type SFs exhibited the most significant impact on flexural strength, closely followed by copper-plated SFs. The difference in the contribution to flexural strength between these two types of SFs was merely 2.86%. The absence of coarse aggregate in the mortar specimen results in reduced friction between the SF and the matrix. However, the end-hook type SF, characterized by a specific bending angle at both ends of the hook, enhances its friction with the matrix. Regarding copper-plated fibers, the characteristic of a higher density of SFs per unit volume plays a role. Consequently, the end-hook type SF contributes the most, with the contribution values showing a closer proximity between copper-plated SFs and the endhook type SFs. In Figure 12, the impact of factor B (SF dosage) on the flexural strength of mortar specimens is

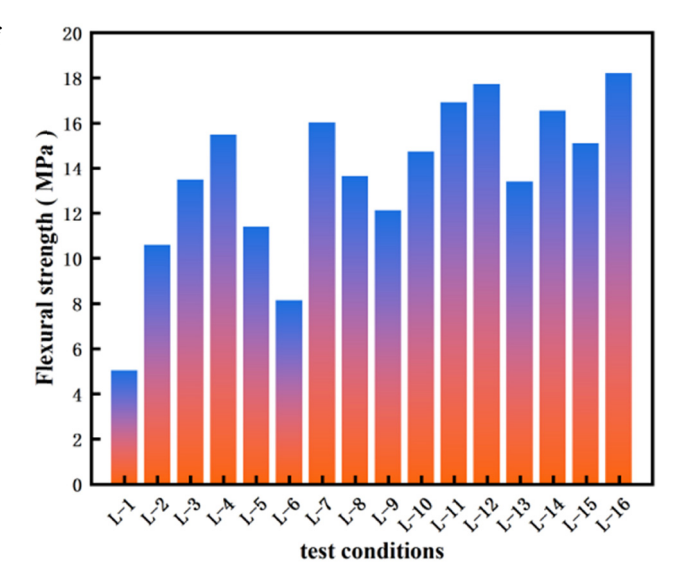


Figure 11: Flexural strength of complex-phase conductive fiber mortar.

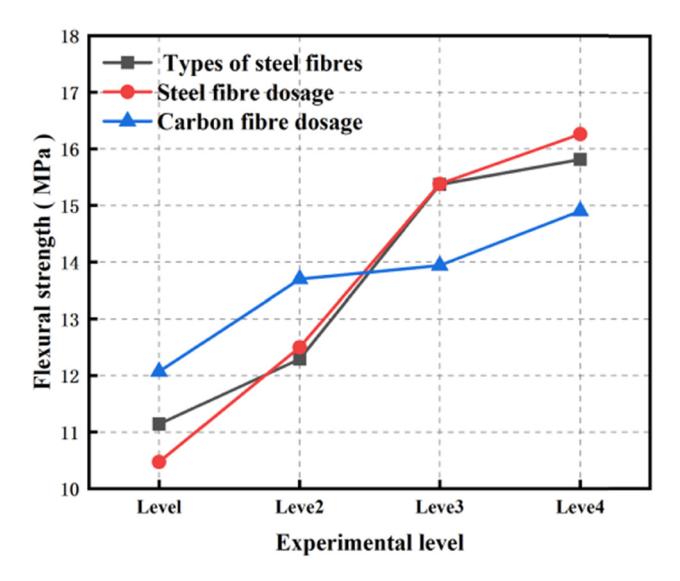


Figure 12: Orthogonal test factor analysis.

evident. The flexural strength exhibits a consistent upward trend with the increase in SF dosage. In other words, as the SF dosage increases, the flexural strength also gradually rises. The flexural strength of the mortar specimen reaches its maximum value when the SF dosage is 1.25%. This indicates that within a certain range, an increased dosage of SF corresponds to higher flexural strength in the fiber mortar specimen, establishing a positive and significant relationship between the two. From Figure 12 and Table 6, it is evident that factor C (CF dosage) has the smallest extreme difference, indicating the least impact of CF dosage on the flexural strength of the mortar specimens. With the increase in CF dosage, the flexural strength gradually increases, reaching its peak when the dosage of CF is 0.48%. The performance of CFs in concrete and mortar specimens differs, with the effect of CFs on flexural strength in mortar specimens being more pronounced. This is attributed to the absence of coarse aggregate incorporation, allowing the short-cut CFs to form a more thorough bond with the mortar specimen matrix, thereby fully leveraging their high resilience modulus.

#### 3.1.2 Analysis of variance for flexural strength

The variance analysis method in the orthogonal test was employed to analyze the results of the flexural strength test for composite conductive fiber mortar. The analysis results are presented in Table 7.

As indicated in Table 7, there are two significant factors and one non-significant factor. The significant factors have a significance level (P) less than 0.05. Factor C (CF admixture) is a non-significant factor, with its significance level (P) greater than 0.05 [40]. Given that the P-value of factor B is lower than the P-value of factor A, it indicates that the impact of factor B (SF dosage) on flexural strength is more pronounced than the impact of factor A (SF type) on flexural strength. Factor C has the least influence on flexural strength, indicating that the contribution of CF content to flexural strength is minimal. As the dosage of SFs increases, the tensile strength of the complex phase conductive cementitious materials also increases due to the high modulus of the SFs. With higher SF content, the tensile strength increases due to enhanced fiber bridging. However, the tensile strain capacity at peak stress decreases [41,42]. It can be concluded that the results of variance analysis are in line with the findings of the range analysis.

#### 3.1.3 Flexural strength matrix analysis

A matrix analysis was conducted on the flexural strength test results of the complex-phase conductive fiber mortar using the analytical method in the orthogonal test. The summarized results are presented in Table 8.

According to the results of matrix analysis, the weight values of its three factors are 0.3511, 0.4353, and 0.2136, respectively. Based on the magnitude of the weight values, the order of significance of the factors can be directly derived as B > A > C. Further analysis results in the optimal combination as A4B4C4. The matrix analysis method remains unaffected by subjective factors throughout the entire evaluation cycle, ensuring the high reliability of the research results. Through range, variance,

Table 7: Summary of variance analysis results

Test name	Factor	Sum of squared deviations	Degree of freedom	Mean square	<i>f</i> ratio	<i>P</i> ratio
Flexural strength	A (SF type)	63.25	3	21.08	10.16	0.0443
	B (SF dosage)	84.93	3	28.31	13.64	0.0297
	C (CF dosage)	16.64	3	5.55	2.67	0.2204
	Error	6.22	3	2.07		

Table 8: Summary of matrix analysis results

Level of factors	Flexural streng	th
	Weighted calculated value	Grand total
A1(SFA)	0.0716	0.3511
A2(SFB)	0.0790	
A3(SFC)	0.0988	
A4(SFD)	0.1017	
<i>B</i> 1(0.35%)	0.0835	0.4353
B2(0.65%)	0.0996	
B3(0.95%)	0.1226	
B4(1.25%)	0.1296	
C1(0.12%)	0.0472	0.2136
C2(0.24%)	0.0536	
C3(0.36%)	0.0545	
C4(0.48%)	0.0583	

and matrix analysis, it is observed that the impact of various factors on the flexural strength of mortar test blocks is consistent. The test results have undergone the steps of analysis, verification, and re-verification, leading to greater accuracy in the findings.

#### 3.2 Conductivity orthogonal test results

The electrical conductivity (volume resistivity) of composite conductive fiber mortar undergoes scrutiny through range analysis, variance analysis, and matrix analysis. The discussion delves into the impact of various factors on the volume resistivity of composite conductive fiber mortar. A comprehensive analysis of the influence of different factors and levels on the test index is conducted, leading to the determination of the optimal combination of factors and levels. Table 9 summarizes the orthogonal test results for the volume resistivity of composite conductive fiber mortar.

#### 3.2.1 Volume resistivity polarization analysis

The results of volume resistivity under the 28-days orthogonal test of complex-phase fiber mortar are depicted in

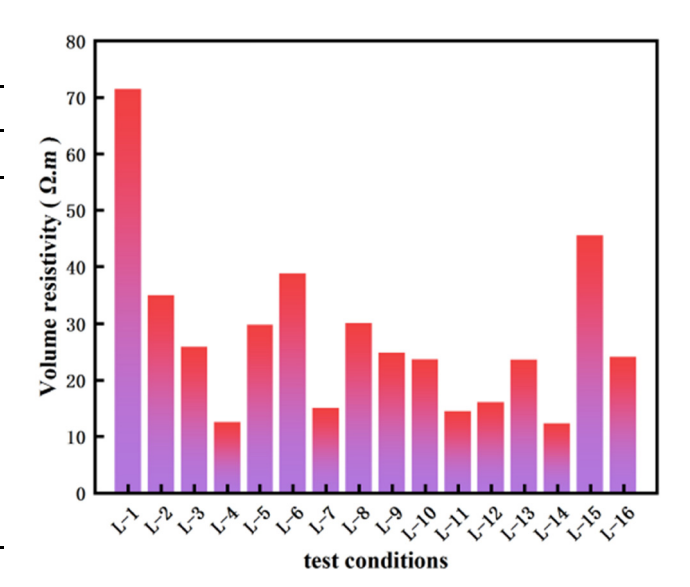


Figure 13: Flexural strength of complex phase conductive fiber mortar.

**Table 10:** Summary of the results of the extreme variance analysis

Parameters	<i>A</i> (SF type)	<i>B</i> (SF dosage)	C (CF dosage)	Blank column
k1	36.14	37.39	37.15	28.62
k2	28.35	27.36	31.50	25.70
<i>k</i> 3	19.66	25.13	23.20	25.78
<i>k</i> 4	26.31	20.59	18.62	30.36
Polar deviation <i>R</i>	16.48	16.79	18.53	4.66

Figure 13. The test outcomes underwent characterization through polar analysis, and the analysis results are presented in Table 10.

As observed in Table 10, the corresponding extreme values for the three factors (A, B, and C) are 21.28, 25.01, and 28.02, respectively. The relationship between the effect of each factor on resistivity is as follows: (C) CF doping > (B) SF doping > (A) SF type. The better the conductivity of the complex-phase conductive fiber mortar, the smaller its resistivity value. The optimized level combination is

Table 9: Summary of volume resistivity test results for complex-phase conductive fiber mortar

Test conditions	Volume resistivity (Ω·m)						
L-1	71.47	L-5	29.72	L-9	24.79	L-13	23.56
L-2	34.88	L-6	38.76	L-10	23.60	L-14	12.20
L-3	25.80	L-7	14.90	L-11	14.34	L-15	45.48
L-4	12.42	L-8	30.02	L-12	15.92	L-16	24.02

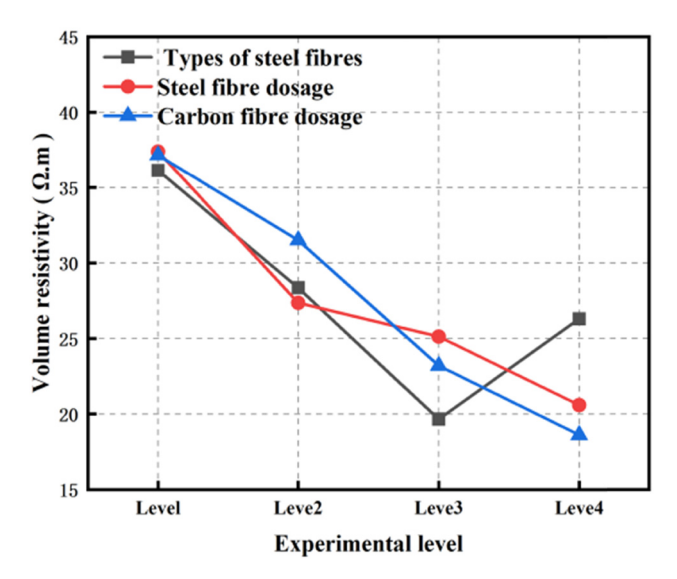


Figure 14: Orthogonal test factor analysis.

A3B4C4, indicating that the use of copper-plated SFs at a dosage of 1.25% and CFs at a dosage of 0.48% has the most significant impact on reducing mortar resistivity, resulting in the highest degree of resistivity reduction and the best electrical conductivity.

To better illustrate the influence of each factor on the volume resistivity of the mortar test block at different levels, an effect line chart has been created to represent the average value of the results obtained at each level, as depicted in Figure 14.

As observed in Figure 14, each type of SF has a varying impact on resistivity, with copper-plated (SFC) concrete exhibiting the lowest resistivity and superior electrical conductivity. The rationale behind this observation is that the copper-plated SF has a shorter and finer length, resulting in a higher number of fibers per unit volume, facilitating interlacing between the fibers. As seen in Figure 14, the resistivity tends to decrease with the increase in SF and CF doping. The resistivity was lower when SF doping was 1.25%, showing a decrease of 44.93% relative to the doping level of 0.35%. Similarly, when CF doping was 0.48%, the resistivity decreased by 50.12% relative to the doping of 0.12%. The reason for this is that with increased doping of conductive phases, the structure of the

Table 12: Summary of results of matrix analysis

Level of factors	Flexural streng	th
	Weighted calculated value	Grand total
A1(SFA)	0.0580	0.3181
A2(SFB)	0.0739	
A3(SFC)	0.1065	
A4(SFD)	0.0797	
B1(0.35%)	0.0571	0.3241
B2(0.65%)	0.0781	
B3(0.95%)	0.0850	
B4(1.25%)	0.1038	
C1(0.12%)	0.0619	0.3577
C2(0.24%)	0.0730	
C3(0.36%)	0.0992	
C4(0.48%)	0.1235	

conductive backbone improves, leading to enhanced electrical properties in both optimal and ideal scenarios.

#### 3.2.2 Analysis of variance

The variance analysis method of orthogonal test was employed to analyze the variance of the volume resistivity test results of the composite conductive fiber mortar. The analysis results are presented in Table 11.

It can be observed from Table 11 that the significance levels (P) of factor B and factor C are 0.0472 and 0.0309, respectively, both of which are less than 0.05, indicating that both are significant factors. Among them, CF content (C) is a highly significant influencing factor, while SF type (B) is not a significant influencing factor. It is evident that the results of this analysis align with the findings of the range analysis.

#### 3.2.3 Matrix analysis

Matrix analysis was conducted on the volume resistivity test results of the complex-phase conductive fiber mortar using the analytical method in the orthogonal test, and the results are summarized in Table 12.

Table 11: Summary of variance analysis results

Test name	Factor	Sum of squared deviations	Degree of freedom	Mean square	<i>f</i> ratio	<i>P</i> ratio
Volume resistivity	A (SF type)	552.61	3	184.20	8.86	0.0531
	B (SF dosage)	604.09	3	201.36	9.69	0.0472
	C (CF dosage)	825.25	3	275.08	13.24	0.0309
	Error	62.34	3	20.78		

From Table 12, it can be observed that the sum of the weight values for the three factors (A, B, and C) is 0.3181, 0.3241, and 0.3577, respectively. It can be concluded that the factors affecting the electrical resistivity of the complexphase conductive fiber mortar are, in descending order, C > B > A. Among the four levels of SF type (A), A3 has the highest influence weight; among the four levels of SF doping (B), B4 has the highest influence weight; and among the four levels of CF doping (C), C4 has the highest influence weight. Comparing the weights between the levels, it can be seen that the optimal combination scheme is A3B4C4, which means copper-plated SF, with a SF content of 0.125%, and a CF content of 0.48% should be added. Through matrix analysis, the above range and variance analysis are further verified, and the conclusions of the three analysis methods are consistent with each other.

## 3.3 Conductive fiber mortar temperature rise test study

# 3.3.1 Analysis of the amount of change in temperature of conductive fiber mortar at elevated temperatures

In the heating test of complex-phase conductive fiber mortar, the temperature data from four measurement points (*T*1, *T*2, *T*3, and *T*4) were averaged to obtain the maximum values, minimum values, and the differences, as shown in Table 13.

### 3.3.2 Conductive fiber mortar temperature rise test analysis

Zhou [43] discovered that under the same voltage, the conductivity of the test specimen is enhanced, resulting in lower resistance. Consequently, the heating power of the test specimen increases, leading to a greater amount of temperature change. The temperature rise test exhibits a certain correlation with conductivity; the higher the conductivity, the greater the temperature rise. In this study, orthogonal analysis of electrical conductivity reveals that the order of influence of the three factors on electrical conductivity is as follows: (C) CF content > (B) SF content > (A) SF type. The SF type factor has the lowest influence and is the least significant factor. Therefore, the influence of the SF type factor is ignored, and only two factors, CF doping and SF doping, are considered for visual analysis of the data from the 16 sets of temperature rise tests under working conditions. Utilizing the data from Table 13, we can draw intuitive bar graphs to analyze the temperature difference in the complex-phase

**Table 13:** Temperature rise of complex phase conductive fiber mortar

Test conditions	Temperature initial value (°C)	Temperature final value (°C)	Temperature difference (°C)
L-1	28.75	32.55	3.80
L-2	24.35	30.75	6.40
L-3	29.30	41.15	11.85
L-4	28.83	57.63	28.80
L-5	30.10	35.38	5.28
L-6	30.08	34.33	4.25
L-7	28.05	49.40	21.35
L-8	31.48	51.70	20.23
L-9	27.45	36.13	8.68
L-10	30.03	46.38	16.35
L-11	25.90	32.63	6.73
L-12	27.60	35.00	7.40
L-13	27.30	41.38	14.08
L-14	30.13	40.55	10.43
L-15	27.95	35.10	7.15
L-16	28.05	34.83	6.78

conductive fiber mortar. The following figures provide a visual analysis of the temperature difference during the warming process of the complex-phase conductive fiber mortar, as shown in Figures 15 and 16.

Figure 15 illustrates the impact of CF doping on the temperature rise test. It is evident that, with a constant SF doping level, the temperature difference during the heating process increases with higher CF doping levels, indicating a proportional increase in temperature rise. The maximum temperature difference in the warming test is achieved when SF doping is at 1.25% and CF doping is at 0.48%, signifying an optimal combination for the highest temperature rise during the test. Figure 16 illustrates the impact of SF dosage on the temperature rise test. It is evident that, with a constant CF dosage, the temperature difference gradually increases as the SF dosage increases. After comparing Figure 15 with Figure 16, it is found that the magnitude of change is more pronounced with the increase in CF doping when the SF doping is constant. Conversely, when the CF doping is constant, with the gradual increase in SF doping, the magnitude of change is relatively flat. The reason is that the conductivity of CF is greater than that of SF. With the incorporation of CF, the conductivity is greatly improved, leading to a noticeable change in temperature rise.

#### 3.4 Conductive mortar current change rate

To investigate the relationship between the rate of current change and the change in temperature rise of the

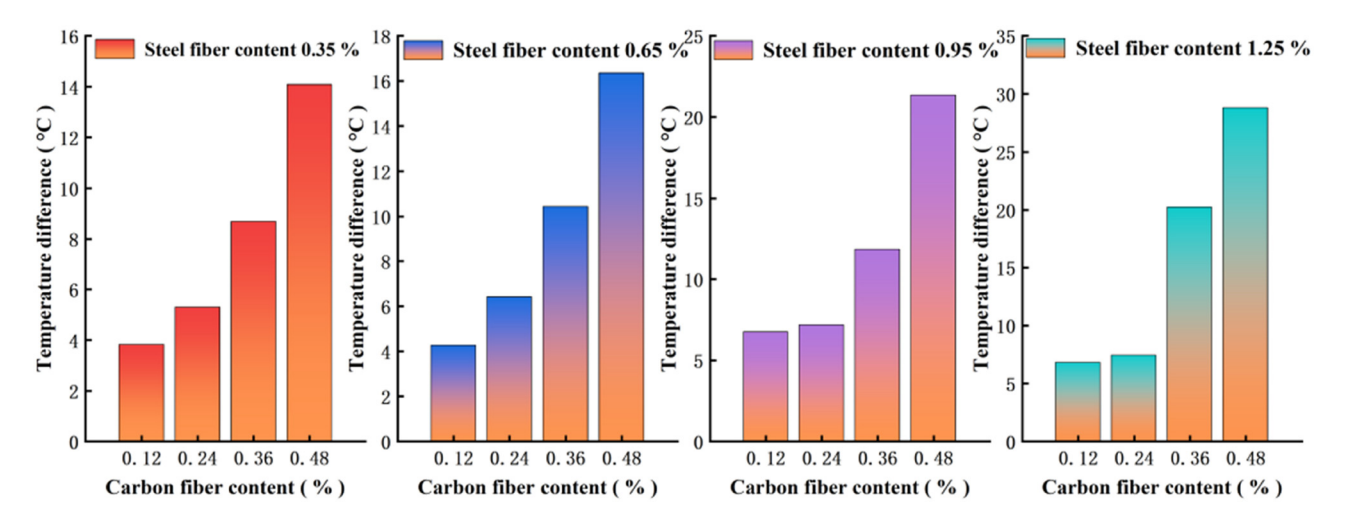


Figure 15: Effect of CF doping on warming test.

composite conductive fiber mortar, a data analysis was conducted on the obtained test data. The average temperature data obtained from the four temperature sensors were utilized. The data for the rate of current change and the change in temperature rise were selected at the 2 min time point to create the relevant line chart. The analysis of the above test leads to the conclusion that the conductivity and temperature rise performance of Case 4 are optimal. Figure 17 illustrates the relationship between the rate of current change, temperature, and time for Case 4.

The red curve in Figure 17 represents the results of the heating test of the composite fiber conductive paste test block in continuous power mode for 120 min. Due to the 48 mortar specimens subjected to a 2 h warming test for each power condition, the average values were taken for each condition from three mortar specimens. Due to the varying sensitivity of the test instrument, slight differences

in the initial temperature of individual mortar specimens were observed, all falling within the error range. As seen from the figure, the heating curve of the complex fiber mortar specimen can be divided into two stages. The first stage of heating is faster, mainly evidenced by a larger temperature increase within the same energization time. In the second stage, the temperature rise gradually slowed down, and the curve approached a plateau, resulting in a relatively stable temperature. This is because at a constant temperature, the applied electric power is equal to the rate of heat exchange between the specimen and the environment, reaching a state of thermal equilibrium.

Figure 17 shows the red and blue curves representing the results of the conductive mortar electro-thermal performance test, illustrating the relationship between the rate of change of current and the amount of change in warming temperature. From the figure, it can be observed

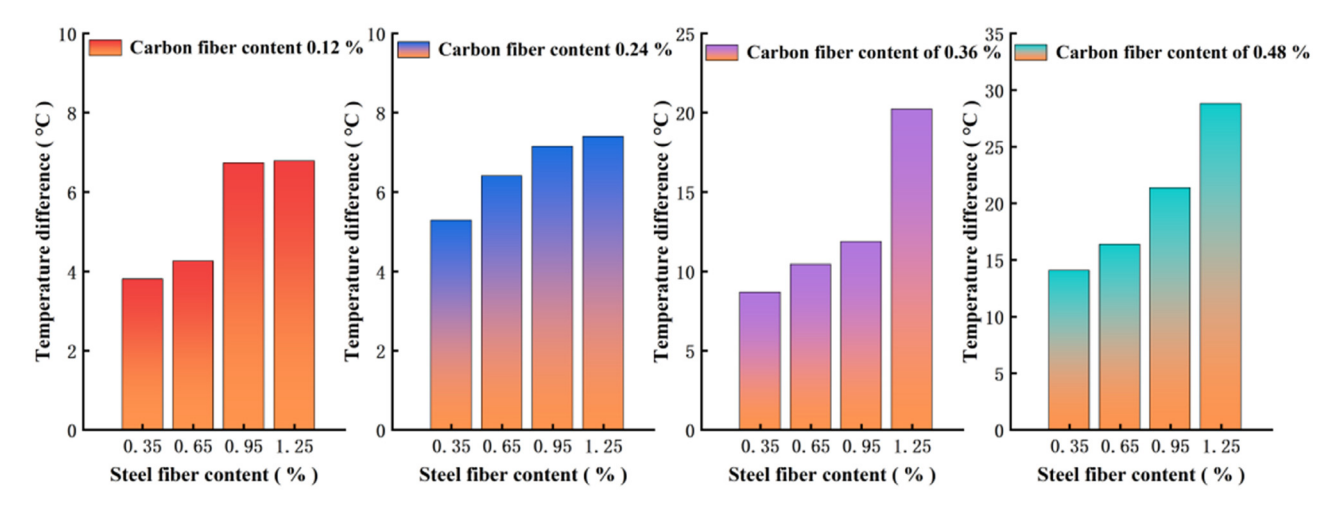
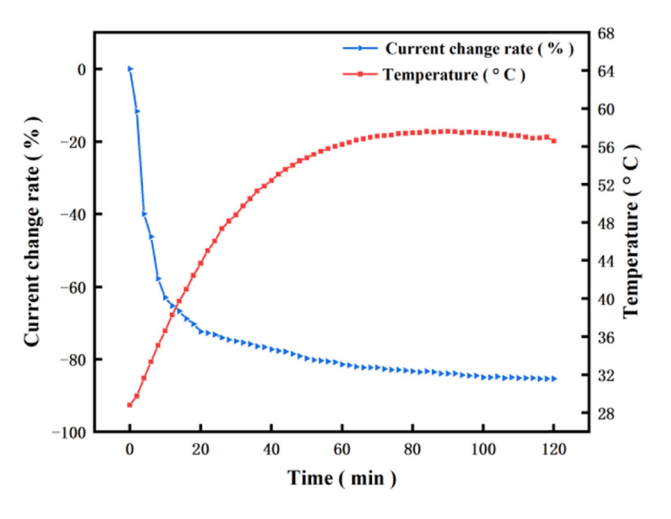


Figure 16: Effect of SF dosage on warming test.



**Figure 17:** The change curve of current change rate and temperature with time.

that the relationship between the rate of change of current and temperature can be divided into two stages. In the first stage, the complex-phase conductive fiber mortar exhibits a decreasing trend in current with the increase in temperature. Given that the voltage is constant, it can be inferred that the resistivity of the complex-phase conductive fiber mortar gradually increases with the rise in temperature. The phenomenon of resistivity increasing with temperature is referred to as the positive temperature coefficient (PTC) effect. Under specific conditions, the resistivity of all specimens increases within 30 min, a phenomenon known as the PTC effect [44]. At higher voltages, the PTC effect dominates in all specimens, while at lower input voltages, the negative temperature coefficient (NTC) effect dominates [45]. Both the PTC effect and the NTC effect are attributed to thermal expansion, as reported by Luo et al. [46]. It can be inferred from this that, since a 64 V DC voltage is used in this work, under energized conditions, for a very short period of time, first, thermal expansion causes the NTC effect. Subsequently, thermal expansion quickly reaches a certain level, and then the PTC effect occurs. In other words, the PTC effect begins when a high enough degree of thermal expansion is reached [45]. It is only because of the extremely short time to reach sufficient expansion that the PTC effect dominates in this test at the applied voltage. In the second stage of the phenomenon, the current curve and temperature curve of the complex-phase conductive fiber mortar show a gradual smoothing trend. This is due to the fact that the internal circuit that can be connected is basically in a stable state, and the resistivity is no longer decreasing.

As mentioned earlier, when the degree of thermal expansion is below a certain level, the NTC effect occurs due to the lapping of CF and SF and their close proximity to

each other. In contrast, when the thermal expansion of the complex-phase conductive fiber material exceeds a certain value, discontinuities between the CFs occur, leading to the occurrence of PTC. It was found that the coefficient of thermal expansion of cement paste is higher [47,48]. CF is known to have a lower coefficient of thermal expansion than cement mortar and SF. When CF is subjected to temperature, its elongation is more stable than that of other materials, and the smaller coefficient of thermal expansion makes it more suitable for environments at both room and elevated temperatures. Hence, CFs exhibit commendable dimensional stability in cementitious materials, even under the demanding conditions of high temperatures. Contrarily, cement paste and SFs are susceptible to the thermal expansion associated with high temperatures. In the case of complex-phase conductive fiber mortar, where the degree of thermal expansion is higher, the discrepancy in expansion coefficients among cement paste, SFs, and CFs can result in discontinuities between the fibers. As the temperature rises, the resistance gradually decreases, manifesting a distinct PTC effect.

#### 4 Conclusion

In this study, the impact of resistivity and flexural strength in complex-phase conductive fiber mortar was investigated through an orthogonal test. A 64 V DC voltage was applied to the electrodes of the conductive fiber mortar, and the continuous recording of specimen temperature during a 2 h energization period was conducted. Warming curves were plotted to examine the current variations throughout the warming process. Simultaneously, the influence of different combinations of fiber types and dosages on the temperature changes over time during mortar warming was also explored. Finally, the electrothermal properties of the complex-phase conductive fiber mortar were investigated in terms of the relationship between temperature and the rate of change of current. The following main conclusions were drawn:

- 1) Based on the results of the orthogonal test on electrical conductivity and mechanical properties, a comprehensive analysis of the significance of each factor was conducted. The optimal combination was identified as *A3B4C4*, indicating that doping copper-plated SFs at 1.25% and CFs at 0.48% has a positive impact on the electrical conductivity, mechanical properties, and electrothermal properties of the composite conductive fiber mortar.
- At a constant voltage, increased fiber doping results in enhanced specimen conductivity, reduced volume

- resistivity, increased heating power, and a greater temperature change.
- 3) The heating curve of the complex fiber mortar specimen can be divided into two stages. The first stage exhibits a faster rate of heating, primarily characterized by a notable increase in temperature within the same energized duration. The second stage involves a gradual slowdown in the heating process, and the curve approaches a plateau, indicating a more stable temperature under continuous energization.
- 4) The relationship between the rate of change of current and temperature can be divided into two phases. In the first phase, the current of the complex-phase conductive fiber mortar tends to diminish as the temperature increases, exhibiting a PTC effect. At higher voltages, the PTC effect dominates in all mortar specimens. In the second phase of the phenomenon, both the current curve and temperature curve of the complex-phase conductive fiber mortar exhibit a gradual flattening trend. This is attributed to the fact that the internal circuit, which can be connected, has essentially stabilized, and the resistivity is no longer decreasing.

**Acknowledgments:** First of all, I thank teacher Li Jiuyang for determining the research direction for me and guiding my experiment. Thanks to Guo Jinpeng, Luo Jingwei, Fan Xinmei and Zhu Yuepeng for helping me complete the experiment. Thank you for your help and support.

**Funding information:** This project is financially supported by the Science and Technology Development Plan of Jilin Province (20210203178SF) and (YDZJ202302CXJD052).

**Author contributions:** Teacher Li Jiuyang determined the research direction and the guidance of the experiment. Wang Zhenwei, designed the experiment and wrote the thesis. Guo Jinpeng, Luo Jingwei, Fan Xinmei, and Zhu Yuepeng, provided help to complete the experiment together. All authors have accepted responsibility for the entire content of this manuscript and approved its submission.

Conflict of interest: The authors state no conflict of interest.

#### References

- Chung, D. D. L. Self-heating structural materials. Smart Materials and Structures, Vol. 13, No. 3, 2004, pp. 562-565.
- Li, H., Q. Zhang, and H. Xiao. Self-deicing road system with a CNFP high-efficiency thermal source and MWCNT/cement-based high-

- thermal conductive composites. Cold Regions Science and Technology, Vol. 86, 2013, pp. 22-35.
- Tuan, C. Y. and S. Yehia. Evaluation of electrically conductive con-[3] crete containing carbon products for deicing. Materials Journal, Vol. 101, No. 4, 2004, pp. 287-293.
- Tuan, C. Y. Conductive concrete for bridge deck deicing and anti-icing. Technical Report, Nebraska Department of Road, No. SPR-PL-1(037): 2004.
- Ding, S., S. Dong, A. Ashour, and B. Han. Development of sensing [5] concrete: Principles, properties and its applications. Journal of Applied Physics, Vol. 126, No. 24, 2019.
- Fan, L., W. Meng, L. Teng, and K. H. Khayat. Effect of steel fibers with galvanized coatings on corrosion of steel bars embedded in UHPC. Composites Part B: Engineering, Vol. 177, 2019, id. 107445.
- Demircilioglu, E., E. Teomete, and O. E. Ozbulut. Strain sensitivity of steel-fiber-reinforced industrial smart concrete. Journal of Intelligent Material Systems and Structures, Vol. 31, No. 1, 2020, pp. 127–136.
- Tuan, C. Y. Electrical resistance heating of conductive concrete containing steel fibers and shavings. Materials Journal, Vol. 101, No. 1, 2004, pp. 65-71.
- Santillán, N., S. Speranza, J. M. Torrents, and I. Segura. Evaluation [9] of conductive concrete made with steel slag aggregates. Construction and Building Materials, Vol. 360, 2022, id. 129515.
- [10] Ding, Y., Y. Yang, R. Liu, T. Xiao, and J. Tian. Study on pressure sensitivity of smart polymer concrete based on steel slag. Measurement, Vol. 140, 2019, pp. 14-21.
- [11] Vaidya, S. and E. N. Allouche. Strain sensing of carbon fiber reinforced geopolymer concrete. Materials and Structures, Vol. 44, No. 8, 2011, pp. 1467-1475.
- Wang, Y. Y. and L. Q. Zhang. Development of self-sensing cementitious composite incorporating hybrid graphene nanoplates and carbon nanotubes for structural health monitoring. Sensors and Actuators A: Physical, Vol. 336, 2022, id. 113367.
- [13] Luo, B. and J. Dong. Optimizing piezoresistivity of alkaliactivated mortar using carboxylated multi-walled carbon nanotubes/basalt fibers. Materials Letters, Vol. 329, 2022, id. 133151.
- [14] Song, F., Q. Chen, Z. Jiang, X. Zhu, B. Li, B. He, et al. Piezoresistive properties of ultra-high-performance fiber-reinforced concrete incorporating few-layer graphene. Construction and Building Materials, Vol. 305, 2021, id. 124362.
- [15] Lu, D., D. Wang, and J. Zhong. Highly conductive and sensitive piezoresistive cement mortar with graphene coated aggregates and carbon fiber. Cement and Concrete Composites, Vol. 134, 2022, id. 104731.
- [16] Liu, L., J. Xu, T. Yin, Y. Wang, and H. Chu. Improving electrical and piezoresistive properties of cement-based composites by combined addition of nano carbon black and nickel nanofiber. Journal of Building Engineering, Vol. 51, 2022, id. 104312.
- Liang, J. and Q. Yang. Prediction of over-permeability threshold of conductive polymer composites. Journal of South China University of Technology (Natural Science Edition), Vol. 8, 2007, pp. 80-82 + 88.
- Guan, X., J. Ou, B. Han, M. Zhao, L. Wang, F. Zhang, et al. Research and progress of carbon fiber mechanosensitive concrete materials. Journal of Harbin Architecture University, Vol. 6, 2002, pp. 55-59.
- [19] Tang, Z., Z. Li, Z. Hou, X. Wang, Y. Liu, M. Chen, et al. Analysis of snow and ice melting mechanism of conductive concrete. Concrete, Vol. 7, 2001, pp. 8-11.
- [20] Sun, M., Z. Li, and Q. Mao. Research on the electro-thermal characteristics of CFRC. Journal of Wuhan University of Technology, Vol. 2, 1997, pp. 72-74 + 77.18.

- [21] Zhu, S. and D. D. L. Chung. Numerical assessment of the methods of measurement of the electrical resistance in carbon fiber reinforced cement. *Smart Materials and Structures*, Vol. 16, No. 4, 2007, pp. 1164–1170.
- [22] Kim, H. K., I. W. Nam, and H. K. Lee. Enhanced effect of carbon nanotube on mechanical and electrical properties of cement composites by incorporation of silica fume. *Composite Structures*, Vol. 107, 2014, pp. 60–69.
- [23] Nam, I. W., H. K. Kim, and H. K. Lee. Influence of silica fume additions on electromagnetic interference shielding effectiveness of multi-walled carbon nanotube/cement composites. *Construction and Building Materials*, Vol. 30, 2012, pp. 480–487.
- [24] Zhou, T., Y. Sun, and Y. Peng. Piezoresistive response of mechanically sensitive concrete composites with compounded functional fillers. *Journal of Materials Science and Engineering*, Vol. 39, No. 5, 2021, pp. 763–767.
- [25] Belli, A., A. Mobili, T. Bellezze, and F. Tittarelli. Commercial and recycled carbon/steel fibers for fiber-reinforced cement mortars with high electrical conductivity. *Cement and Concrete Composites*, Vol. 109, 2020, id. 103569.
- [26] Reza, F., J. A. Yamamuro, and G. B. Batson. Electrical resistance change in compact tension specimens of carbon fiber cement composites. *Cement and Concrete Composites*, Vol. 26, No. 7, 2004, pp. 873–881.
- [27] Chiarello, M. and R. Zinno. Electrical conductivity of self-monitoring CFRC. Cement and Concrete Composites, Vol. 27, No. 4, 2005, pp. 463–469.
- [28] Li, G.-Y. and P.-M. Wang. Mechanical properties and microstructure of carbon nanotube-cementitious composites. *Journal of Silicates*, Vol. 1, 2005, pp. 105–108.
- [29] Ba, H. and X. Gao. Research on early cracking control measures of high performance concrete. *Journal of Harbin Architecture University*, Vol. 5, 2002, pp. 77–80.
- [30] Huang, L., Z. Li, and X. Song. Study on the durability of carbon fiber concrete under repeated temperature changes. *Concrete*, Vol. 12, 2002, pp. 35–37.
- [31] Chen, P. and D. D. L. Chung. Low-drying-shrinkage concrete containing carbon fibers. *Composites Part B: Engineering*, Vol. 27, No. 3, 1996, pp. 269–274.
- [32] GB 175-2007, General purpose silicate cement.
- [33] JGJ 52-2006, Standard for quality and test methods of sand and gravel for ordinary concrete.
- [34] GB/T 39147-2020, Steel fibers for concrete.
- [35] Yuan, L. Experimental study on force electrical properties of carbon fiber smart concrete, Doctoral dissertation, Zhengzhou University, Zhengzhou, China, 2012.

- [36] Wang, L., H. Du, and X. Liu. Effect of mixed fibers on the pressuresensitive properties of activated powder concrete. *Concrete*, Vol. 1, 2021, pp. 66–69.
- [37] DL/T 5126-2001, Test procedure for polymer modified cement mortar.
- [38] Qin, R. Research on the conductive, pressure-sensitive and electrothermal properties of multi-scale carbon-based cement composites, Doctoral dissertation, Harbin Institute of Technology, Harbin, China, 2014.
- [39] Liu, Z. Research on mechanical, electrical and pressure-sensitive properties of complex-phase conductive fiber concrete, China University of Mining and Technology, Xuzhou, 2022.
- [40] Abdellatief, M., W. E. Elemam, H. Alanazi, and A. M. Tahwia. Production and optimization of sustainable cement brick incorporating clay brick wastes using response surface method. *Ceramics International*, Vol. 49, No. 6, 2023, pp. 9395–9411.
- [41] Abdellatief, M., M. A. Elrahman, G. Elgendy, G. Bassioni, and A. M. Tahwia. Response surface methodology-based modelling and optimization of sustainable UHPC containing ultrafine fly ash and metakaolin. *Construction and Building Materials*, Vol. 388, 2023, id. 131696.
- [42] Tahwia, A. M., A. M. Heniegal, M. Abdellatief, B. A. Tayeh, and M. A. Elrahman. Properties of ultra-high performance geopolymer concrete incorporating recycled waste glass. *Case Studies in Construction Materials*, Vol. 17, 2022, id. e01393.
- [43] Zhou, T. Research on mechanosensitivity of cementitious materials with compounded functional fillers, Jiangsu University, Zhenjiang, 2020.
- [44] He, X. J., J. H. Du, Z. Ying, H. M. Cheng, and X. J. He. Positive temperature coefficient effect in multiwalled carbon nanotube/high-density polyethylene composites. *Applied Physics Letters*, Vol. 86, No. 6, 2005, id. 062112.
- [45] Kim, G. M., F. Naeem, H. K. Kim, and H. K. Lee. Heating and heat-dependent mechanical characteristics of CNT-embedded cementitious composites. *Composite Structures*, Vol. 136, 2016, pp. 162–170.
- [46] Luo, Y., G. Wang, B. Zhang, and Z. Zhang. The influence of crystalline and aggregate structure on PTC characteristic of conductive polyethylene/carbon black composite. *European Polymer Journal*, Vol. 34, No. 8, 1998, pp. 1221–1227.
- [47] Meng, F., X. Zhang, R. Li, J. Zhao, X. Xuan, X. Wang, et al. Electroinduced mechanical and thermal responses of carbon nanotube fibers. *Advanced Materials*, Vol. 26, No. 16, 2014, pp. 2480–2485.
- [48] Sellevold, E. J. and Ø. Bjøntegaard. Coefficient of thermal expansion of cement paste and concrete: Mechanisms of moisture interaction. *Materials and Structures*, Vol. 39, 2006, pp. 809–815.